Thermal and hydraulic modelling of road tunnel joints

Cédric Hounyevou Klotoé[1], François Duhaime[1], Lotfi Guizani[1]

[1] Département de génie de la construction, École de technologie supérieure, Montréal, Québec, Canada

Abstract:

This paper focuses on the use of COMSOL Multiphysics to develop a 2D numerical model of expansion joints for road tunnels. The model was developed using the coefficient form PDEs interface. The model includes water and energy conservation equations. It takes into account the influence of temperature on liquid water saturation and hydraulic conductivity. Under proper boundary conditions, the model allows the temperature, pressure and seepage velocity fields around the joint to be evaluated. The model also allows solutions for different expansion joint problems to be tested. Examples of solutions to prevent the formation of ice in the expansion joints during winter are presented. The model also shows how the temperature gradient close to the joints can be used to estimate their permeability.

Keywords: Thermo-hydraulic phenomena, tunnel, expansion joints

1. Introduction

Expansion joints are often weak links for groundwater seepage in older road tunnels. In case of infiltration, a drainage system allows the disposal of groundwater. For tunnels in cold regions, groundwater seepage can lead to the formation of ice stalactites and patches (Figures 1 and 2). These can cause the degradation of concrete and steel structural elements. Ice formation can also have a negative impact on tunnel serviceability.
To understand water infiltration at tunnel joints in cold climates, it is useful to develop numerical models at the joint scale to simulate the coupled phenomena that control seepage and the formation of ice, namely heat transfer, water flow and phase changes. This type of numerical model could for instance be used to validate various solutions for tunnel repairs.
This report first presents a simplified expansion joint model. A 2D COMSOL Multiphysics model is then introduced. The model is then used to show the influence of joint permeability on water infiltration and ice formation.

Figure 1. Pack of ice coming from a joint and spreading onto the walkway [7]

Figure 2. Ice stalactites and ice patches on the ground [7]

2. Simplified model of expansion joints of a road tunnel

Figure 3 presents the geometry of a simplified model of expansion joints for road tunnels. This model corresponds to a cross section of the concrete tunnel lining at the key of the vault. Soil is present at the tunnel extrados. It is assumed that the expansion joints are located every 15 m along the axis of the road tunnel (x axis on Figure 3). The expansion joint are made of expanded polystyrene. They are traversed by a steel waterstop to control water infiltration.

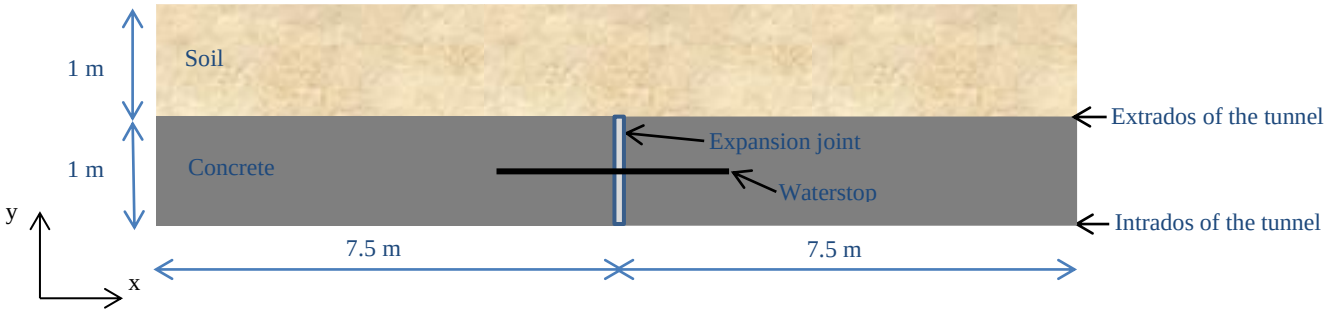

Figure 3. Simplified model of expansion joints for the numerical model

Table 1 presents the dimensions of the expansion joint and waterstop.

Table 1: Dimensions of the expansion joint and waterstop

Materials	Dimensions
Expansion joint	thickness = 0.025 m ; height = 1 m
Waterstop	thickness = 0.025 m ; width = 0.254 m

2.1. Boundaries conditions for the joint model

The boundary conditions for the joint model are presented on Figure 4. At 1 m above of the extrados of the road tunnel, we assume that the:

-temperature of the groundwater is equal to 10 °C;

-pressure head is 10 m.

At the other side of the model that represents the tunnel intrados, the pressure head is null. It is assumed that the air temperature inside the tunnel varies sinusoidally from -25 °C (minimum temperature in winter) to +25 °C (maximum temperature in summer) over a 12 month period (Figure 5). Convection heat transfer is assumed at the interface between air and concrete at the intrados. This boundary condition is determined using the following expression:

$$\emptyset = h\,(T - T_{ext}) \qquad (1)$$

where h is the heat exchange coefficient in W/m². °C; T represents the temperature at the surface of concrete and T_{ext} is the air temperature (Figure 5).

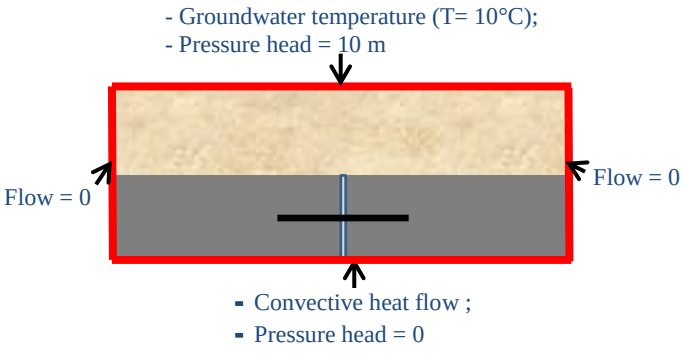

Figure 4. Boundary conditions for the joint model

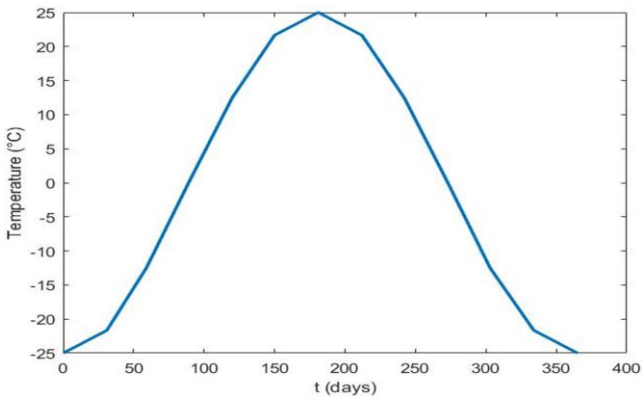

Figure 5. Air temperature as a function of time

2.2. Governing equations of the model

2.2.1. Basic assumptions

As basic assumptions, we have considered that the:

- concrete, soil, expansion joint, and waterstop are porous media saturated with water;
- evaporation of water is ignored, and Darcy's law is suitable to describe the groundwater flow in porous media;
- heat conduction in freezing porous media satisfies Fourier's law.

2.2.2. Heat conduction equation

According to Tan et al. [8], the heat conduction equation deduced from energy conservation in freezing porous media is expressed as:

$$C_v \frac{\partial T}{\partial t} + \rho_l c_l v_l . (\nabla T) + \nabla . (-\lambda_e \nabla T) = 0 \qquad (2)$$

where ρ and c are density and specific heat capacity, respectively. Subscripts s, l and i represent solid matrix, water and ice, respectively. v_l is the seepage velocity of water. Water density is a function of pressure and temperature [2]:

$$\rho_l = \rho_{lo}\left[1 + \alpha_T (T - T_o) + \beta_p (p_l - p_o)\right] \qquad (3)$$

where ρ_{lo} is the density corresponding to the initial pressure p_o and initial temperature T_o; α_T is the thermal expansion coefficient of water related with temperature T; β_p is water compressibility; p_l is water pressure. When $p_o = 101\ kPa$ and $T_o = 20\ °C$, $\alpha_T = (-9T - 80) \times 10^{-6}/°C$ and $\beta_p = 5 \times 10^{-6}/Pa$. The change of water density with temperature when $p_o = 101\ kPa$ is shown in Figure 6.

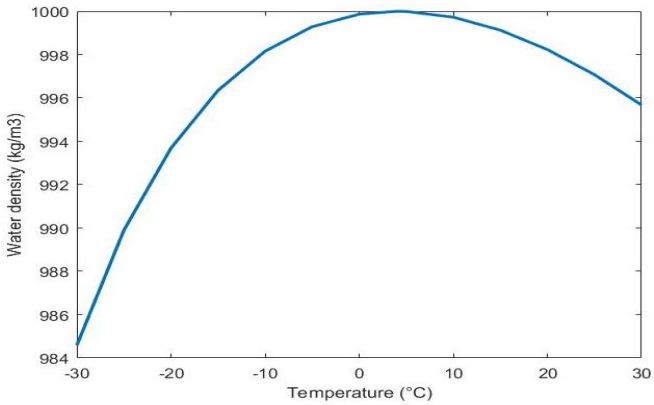

Figure 6. Water density with temperature

λ_e is the effective thermal conduction of the porous media, which depends on the thermal conductivity of its components (solid, unfrozen water, ice), their volumetric fractions and the spatial distribution of its components. It is expressed as follows [2, 9]:

$$\lambda_e = {\lambda_s}^{1-n} {\lambda_l}^{n w_u} {\lambda_i}^{n(1-w_u)} \qquad (4)$$

where n is the porosity and λ is the thermal conductivity. w_u is the unfrozen water content, which could be expressed as an exponential function of temperature [3]:

$$w_u = \begin{cases} e^{M(T-T_m)} & si\ \ T - T_m \leq 0 \\ 1 & si\ \ T - T_m > 0 \end{cases} \qquad (5)$$

where $T_m = 0°C$ is the freezing point of bulk water and M is a parameter related with the distribution of pore radius. C_v is the equivalent volumetric thermal capacity, which can be expressed as follows:

$$C_v = c_s \rho_s (1 - n) + c_l \rho_l w_u n + c_i \rho_i (1 - w_u) n + n \rho_l L_f \frac{\partial w_u}{\partial T} \qquad (6)$$

where L_f is the latent heat of water/ice phase transition.

2.2.3. Continuity equation

The continuity equation of water/ice has been derived by Tan et al. [8] as below:

$$\frac{\partial (\rho_l w_u n)}{\partial t} + \frac{\partial [\rho_i (1 - w_u) n]}{\partial t} + \nabla . (\rho_l v_l) = 0 \qquad (7)$$

Considering that the ice density is constant in the porous media, equation (7) can be expressed as follows:

$$\left(nw_u\beta_p\rho_{lo}\right)\frac{\partial p_l}{\partial t}+\ n\left[\rho_l\frac{\partial w_u}{\partial T}+\rho_i\frac{\partial[(1-w_u)]}{\partial T}\right]\frac{\partial T}{\partial t}+\nabla.(\rho_l v_l)\ =0 \qquad (8)$$

We assume that the water seepage in porous media satisfies Darcy's law as follows:

$$v_l=-\frac{k_r}{\mu_l}k(\nabla p_l-\rho_l g) \qquad (9)$$

where *k* is the intrinsic permeability of saturated porous media before freezing; μ_l is the viscosity of liquid water which can be expressed as a function of freezing temperature *T* [5]:

$$\mu_l=(2.1\times10^{-6})\,exp\left(\frac{1808.5}{273.15+T}\right) \qquad (10)$$

k_r is the relative permeability which can be written as a function of water saturation [8]:

$$k_r=\begin{cases}\sqrt{e^{M(T-T_m)}}\left[1-\left(1-e^{\frac{M(T-T_m)}{z}}\right)^z\right]^2 & if\ \ T-T_m\ \le 0\\ 1 & if\ \ T-T_m>0\end{cases} \qquad (11)$$

where z is a material constant.
In the rest of this report, we will use COMSOL Multiphysics to model the thermo-hydraulic phenomena with water/ice phase change at expansion joint of the road tunnel.

3. Use of COMSOL Multiphysics to model the thermo-hydraulic phenomena with water/ice phase transition at expansion joint of the road tunnel

The principal equations of this 2D numerical model are those define above (2.2.2 and 2.2.3). We have also compared the results of the model with the literature [1].

3.1. Implementation of principal equations in COMSOL Multiphysics

In this section, we have defined two physics related to the thermo-hydraulic phenomena in using the coefficient form PDEs interface of COMSOL whose partial differential equations are expressed as follows:

$$e_a\frac{\partial^2T}{\partial t^2}+d_a\frac{\partial T}{\partial t}\ \nabla.(-c\nabla T\ -\ \alpha T\ +\ \gamma)+\ \beta.\nabla T\ +\ aT\ =\ f \qquad (12)$$

3.2. Heat transfer

For the heat transfer, the equation (2) can be rewritten in COMSOL by analogy with equation (12) as follows:

$$e_a=0;\ \ d_a=C_v=\ c_s\rho_s(1-n)+c_l\rho_l w_u n+c_i\rho_i(1-w_u)n+n\rho_l L_f\frac{\partial w_u}{\partial T};$$
$$c=\ \lambda_e=\ {\lambda_s}^{1-n}{\lambda_l}^{nw_u}{\lambda_i}^{n(1-w_u)};\ \alpha=0\ ;\ \gamma=0\ ;\ a=0\ ;\ f=0\ ;$$
$$\beta=\begin{cases}\beta_x=-\dfrac{\rho_l\,c_l\,k_r\,k}{\mu_l}\left(\dfrac{\partial p_l}{\partial x}\right)\\ \beta_y=-\dfrac{\rho_l\,c_l\,k_r\,k}{\mu_l}\left(\dfrac{\partial p_l}{\partial y}+\rho_l(g)\right)\end{cases}$$

3.3. Hydraulic

For the hydraulic, equation (8) can be rewritten in COMSOL by analogy with equation (12) as follows:

$$e_a=0;\ d_a=nw_u\beta_p\rho_{lo};\ \beta=\ 0;\ a=0;\alpha=0;\ c=\frac{\rho_l k_r k}{\mu_l};\ \gamma=\begin{cases}\gamma_x=0\\ \gamma_y=\dfrac{{\rho_l}^2k_r k}{\mu_l}(-g)\end{cases};$$
$$f=-n\left[\rho_i\frac{\partial(1-w_u)}{\partial T}+\rho_l\frac{\partial w_u}{\partial T}\right]\frac{\partial T}{\partial t}$$

4. Results and discussions

Table 2 in appendix presents the parameters that were used for the calculations in this paper.

4.1. Influence of permeability of the joint on the temperature

The intrinsic permeability of the expanded polystyrene joint was varied to model different joint conditions. Three *k* values were used to represent joints with a high permeability (k = 10^{-10} m²), low permeability (k = 10^{-12} m²) and impermeable joints (k = 10^{-15} m²). Results for each joint condition are presented next.

4.1.1. Permeable joint

Figure 7 presents for the permeable joint, the isotherms, the ice saturation and water saturation obtained winter and summer.

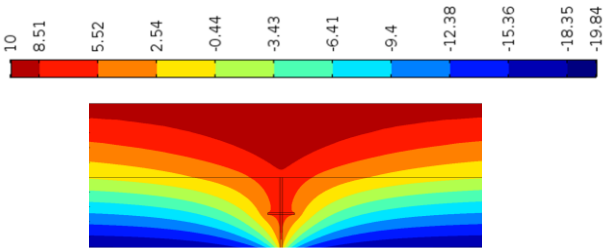

Isotherms in °C at t=31 days (January)

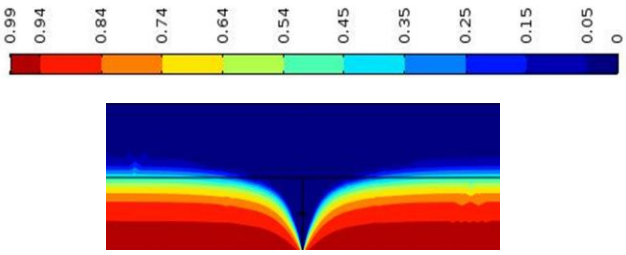

Ice saturation $(1 - w_{n,})$ at t= 31 days (January)

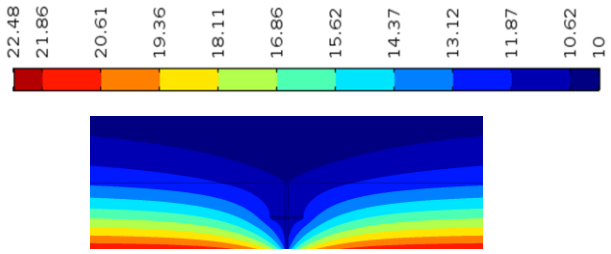

Isotherms in °C at t=181 days (July)

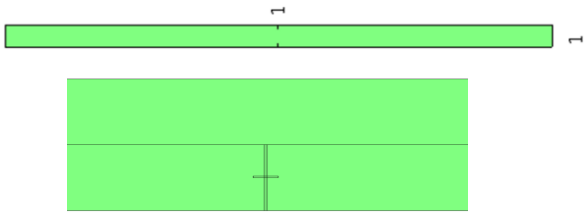

Water saturation (w_u) at t= 181 days (July)

Figure 7. Isotherms, ice saturation and water saturation in the permeable joint model

For the permeable joint, the isotherms obtained in summer and winter have the shape of a drawdown cone with a water temperature inside the tunnel at the joint of 3°C in winter and 10 °C in summer. In winter, the ice saturation shows that the soil and the joint are saturated with water contrary to the concrete which is frozen (impermeable to water) during winter. In summer, all materials (concrete, rock, expansion joint, and waterstop) are saturated with water.

4.1.2. Low-permeability joint

Figure 8 presents for the low-permeability joint, the isotherms, the ice saturation, and water saturation obtained in the model of joint during winter and summer.

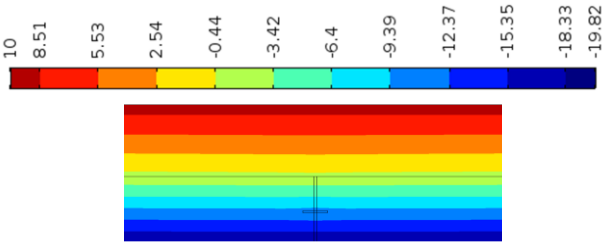

Isotherms in °C at t=31 days (January)

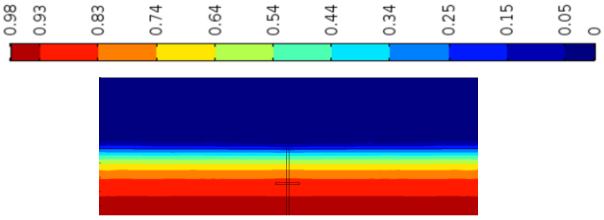

Ice saturation $(1 - w_u)$ at t=31 days (January)

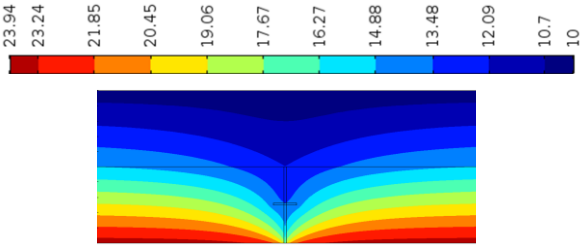

Isotherms in °C at t=181 days (July)

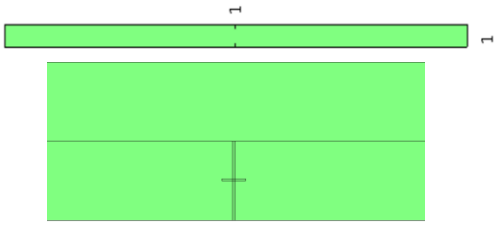

Water saturation (w_u) at t=181 days (July)

Figure 8. Isotherms, ice saturation and water saturation in the low-permeability joint model

In winter, the isotherms are parallel to the tunnel axis with a frozen water temperature inside the tunnel at the joint of -20°C. In summer, the isotherms have the shape of a drawdown cone with a water temperature inside tunnel at the joint of 15°C. Contrary to the previous case, the ice saturation obtained in winter shows that both concrete and the joint are frozen (impermeable to water) unlike the soil which is saturated with water. In summer, all materials (rock, concrete, expansion joint, and waterstop) are saturated with water.

4.1.3. Impermeable joint

Figure 9 presents for the impermeable joint, the isotherms, the ice saturation, and water saturation obtained in the model of joint during winter and summer.

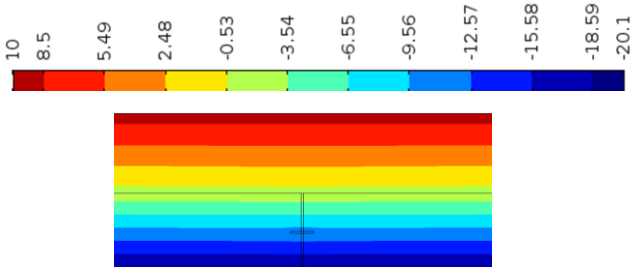

Isotherms in °C at t=31 days (January)

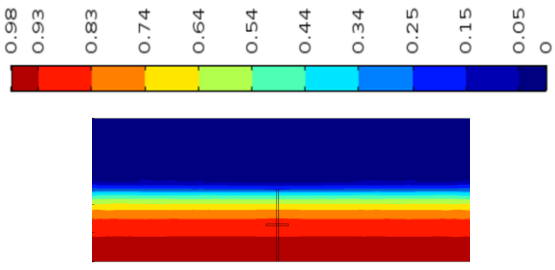

Ice saturation $(1 - w_u)$ at t=31 days (January)

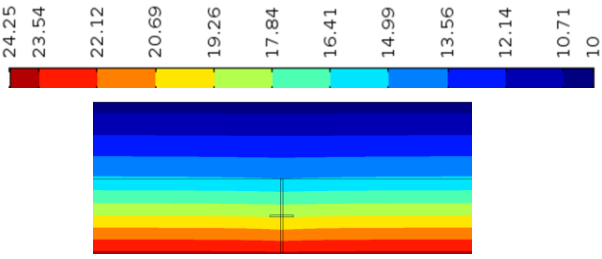

Isotherms in °C at t=181 days (July)

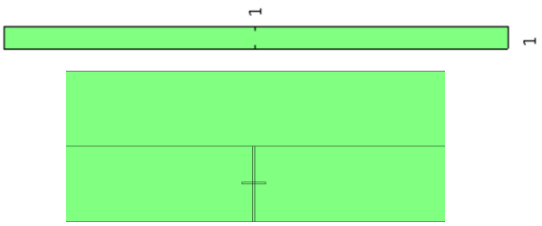

Water saturation (w_u) at t= 181 days (July)

Figure 9. Isotherms, ice saturation and water saturation in the impermeable joint model

During winter, the isotherms are parallel to the tunnel axis with a temperature inside the tunnel at the joint of -20 °C. In summer, this temperature is equal to 24 °C. The ice saturation shows frozen materials (impermeable to water) during winter, whereas liquid water is present during summer.

4.2. Water flow inside the tunnel through the expansion joints

The flow rate in the tunnel is expressed as follows:

$$Q = \left(\frac{k\ k_r(T)\ \rho_l\ g\ A}{\mu(T)}\right) \nabla H \qquad (13)$$

where A is the area of the expansion joint at the intrados; k is the intrinsic permeability of the expansion joint; $k_r(T)$ and $\mu(T)$ are the relative permeability and viscosity of liquid water with temperature; g is the gravity; ρ_l is water density; and H is the hydraulic head.

Figure 10 presents the water flow inside the tunnel for each type of joint (low-permeability and impermeable joints).

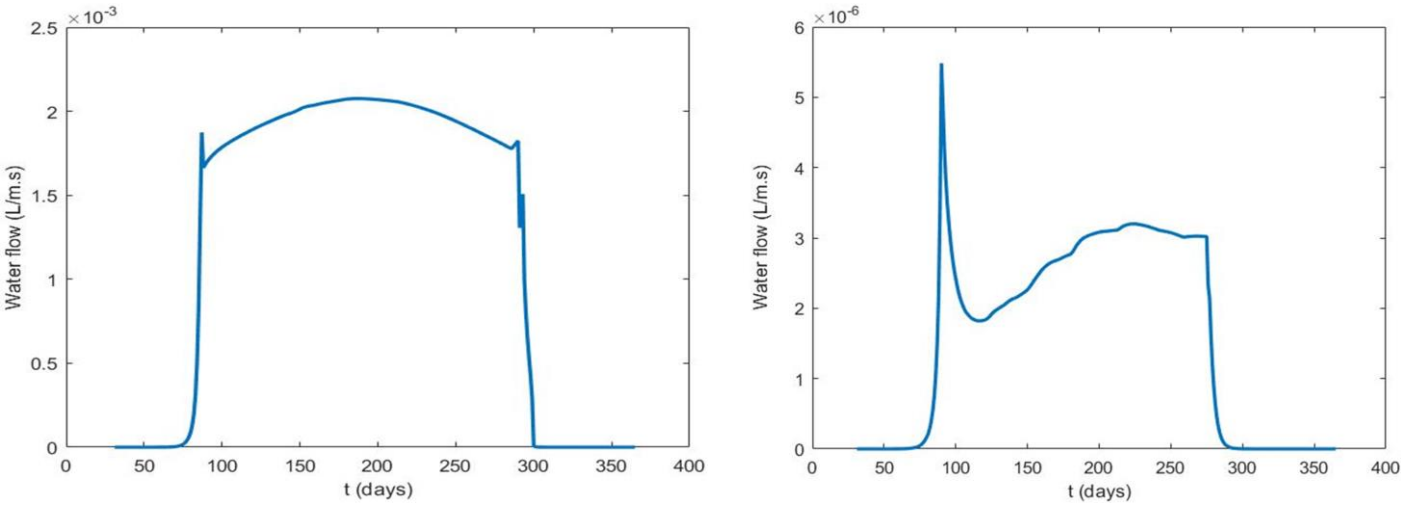

Low-permeability joint

Impermeable joint

Figure 10. Water flow inside the tunnel for each type of joint (low-permeability and impermeable joints)

In the model, the thaw occurs during summer (from t=89 days (April) to t= 273 days (October)) and the freeze during winter (from t= 273 days (October) to 365 days (December) or from t=0 days (January) to t=89 days (April)). For both types of joints (low-permeability joint and impermeable joint), the water flow in winter is equal to zero because of the presence of ice (impermeable to water). The flow rate increases during summer for both joints. At t=89 days, it is equal to respectively 1.68 x 10^{-3} l/m.s and 5.5 x 10^{-6} l/m.s for the low-permeability and impermeable joints. On the other hand, we observe two sudden changes corresponding to the ice to water phase change at t=89 days (April) and the opposite phase change (water to ice) at t=273 days (October) for both joints.

5. Examples of solutions

The model can be used to validate different solutions meant to decrease water infiltration through permeable joints. A decrease in water pressure at the extrados applied through controlled drainage is used as an example herein.

Figure 11 presents the isotherms, the ice saturation and water saturation obtained in the model during winter and summer for a pressure head of 1 m. In winter, the isotherms are parallel to the tunnel axis and the whole joint is frozen (impermeable to water). The flow rate is reduced from 7.86 x 10^{-3} l/m.s to zero at t=31 days (January) or t=365 days (December) for the permeable joint with a pressure head reduced from 10 m to 1 m. In summer, the joint is thawed and the water temperature has the shape of a drawdown cone with a value of 15 °C inside the tunnel at the joint. Also in summer, the flow rate is reduced from 8.6 x 10^{-3} l/m.s to 2.2 x 10^{-3} l/m.s at t=181 days (July) for the permeable joint with a pressure head reduced from 10 m to 1 m. The results obtained show that the reduction of the pressure head allows to reduce the flow rate and to have the whole joint frozen in winter.

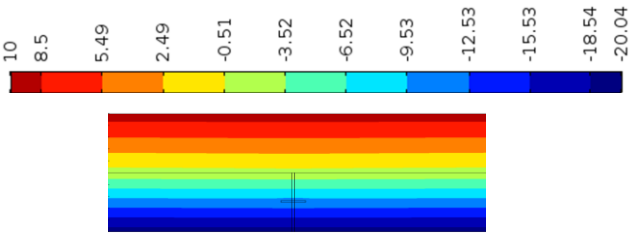

Isotherms in °C at t= 31 days (January)

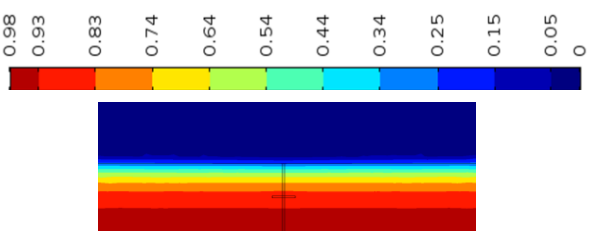

Ice Saturation $(1 - w_{,,})$ at t= 31 days (January)

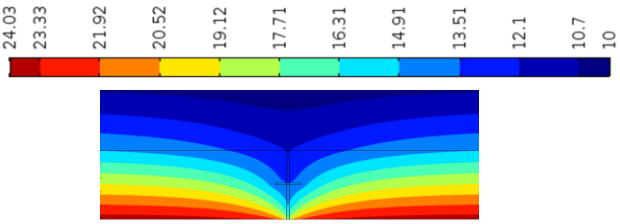

Isotherms in °C at t= 181 days (July)

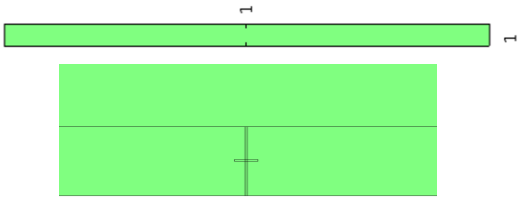

Water Saturation (w_u) at t= 181 days (July)

Figure 11. Isotherms, ice saturation and water saturation obtained in the model of joint for the pressure head of 1 m

6. Conclusion

This paper dealt with the use of COMSOL Multiphysics to develop a 2D numerical model of expansion joints for road tunnels. The model objectives were to simulate the thermo-hydraulic phenomena with water/ice phase change at expansion joint of road tunnels and to model solutions to reduce the groundwater seepage in road tunnels through the expansion joints.

The principal equations of the joint model are based on the continuity equation of water/ice and the heat conduction equation deduced from energy conservation in freezing porous media. Under proper boundary conditions, these equations allow the flow rate and the temperature and pressure fields around each type of joint (permeable, low-permeability, impermeable) to be evaluated for the summer and winter periods. Our results show that the permeable joint is not frozen in winter (saturated with water) unlike the low-permeability and impermeable joints which are frozen (impermeable to water). The evaluation of the flow rate as a function of the permeability of the joint has allowed the time corresponding to the ice/water and water/ice phase change at the expansion joint to be determined. In our case, these phase changes are observed at t= 89 days (April) and t= 273 days (October) for both types of joints (low-permeability and impermeable).

Finally, the modeled solution approach has shown that the reduction of the pressure head allows the permeable joint to freeze in winter, similarly to the low-permeability and impermeable joints.

To improve this paper, it is proposed to take into account the mechanical behavior in this joint model. This physics will allow us to evaluate and analyze the deformations of the joint during the summer and winter periods.

7. References

[1] Huang S, Guo Y, Liu Y, et al (2018). Study on the influence of water flow on temperature around freeze pipes and its distribution optimization during artificial ground freezing, Applied Thermal Engineering, 135, pp 435-445.

[2] Huang S.B, Liu Q.S, Cheng A.P, et al (2018). A fully coupled thermo-hydro-mechanical model including the determination of coupling parameters for freezing rock, International Journal of Rock Mechanics and Mining Sciences, 103, pp 205–2144.

[3] Huang S.B, Liu Q.S, Liu Y.Z, et al (2018). Freezing strain model for estimating the unfrozen water content of saturated rock under low temperature, International Journal of Geomechanics, 18, 04017137, http://dx.doi.org/10.1061/(ASCE)GM.1943-5622.0001057.

[4] Koech R (2015). Water density formulations and their effect on gravimetric water meter calibration and measurement uncertainties, Flow Measurement and Instrumentation, 45, pp 188–197.

[5] Lide D.R (2004). Handbook of Chemistry and Physics, 84th ed, CRC Press Inc, pp 980–981.

[6] Nishimura S, Gens A, Olivella S, et al (2009). THM-coupled finite element analysis of frozen soil: formulation and application, Geotechnique, 59, pp 159–171.

[7] Road tunnel civil engineering inspection guide (2015). Book 2: Catalogue of deteriorations, Centre d'études des tunnels, pp 1-140.

[8] Tan X.J, Chen W.Z, Tian H.M, et al (2011). Water flow and heat transport including ice/water phase change in porous media: numerical simulation and application, Cold Regions Science and Technology, 68, pp 74–84.

[9] Tan X.J, Chen W.Z, Yang D.S, et al (2014). Study on the influence of airflow on the temperature of the surrounding rock in a cold region tunnel and its application to insulation layer design, Applied Thermal Engineering, 67, pp 320–334.

8. Appendix

Table 2. Used parameters for the calculations in the model of joint

Properties	Symbols	Numerical values				Units
		Soil	Concrete	Joint	Waterstop	
Porosity	n	0.065	0.01	0.9	0.01	
Solid matrix density	ρ_s	2600	2300	11.5	7850	kg/m^3
Water density	ρ_l	1000				kg/m^3
Ice density	ρ_i	917				kg/m^3
Specific heat capacity of the solid matrix	c_s	851	880	1450	475	J/kg.K
Specific heat capacity of water	c_l	4180				J/kg.K
Specific heat capacity of ice	c_i	2100				J/kg.K
Thermal conductivity of the solid matrix	λ_s	2.9	1.8	0.05	44.5	W/m.K
Thermal conductivity of water	λ_l	0.59				W/m.K
Thermal conductivity of ice	λ_c	1.7				W/m.K
Intrinsic permeability	k	1.49 x 10^{-13}	1.84 x 10^{-19}	Variable	10^{-9}	m²
Heat exchange coefficient (air)	h	20				W/m².°C